

Construction of diverse dimensionality in eight coordination polymers of bivalent metal ions using 5-nitroisophthalate and different linear N,N'-donor linkers



Dilip Kumar Maity, Biswajit Bhattacharya, Arijit Halder, Anamika Das, Debajyoti Ghoshal*

Department of Chemistry, Jadavpur University, Jadavpur, Kolkata 700 032, India

ARTICLE INFO

Article history:

Received 22 July 2015

Accepted 4 October 2015

Available online 03 November 2015

Keywords:

Coordination polymers

Single crystal X-ray structures

PXRD and TGA study

Solid state UV–Vis spectra

Photoluminescence study

ABSTRACT

Assembly of 5-nitroisophthalate (nip^{2-}) with first row transition metal salts [Mn(II), Fe(II), Co(II), Zn(II)] in combination with the various neutral auxiliary N,N'-donor linkers, e.g., 2,5-bis-(4-pyridyl)-3,4-diaza-2,4-hexadiene (4-bpdh), 1,3-bis(4-pyridyl)propane (bpp) and 1,4-bis(4-pyridyl)-2,3-diaza-1,3-butadiene (4-bpdb), yielded eight new coordination polymers (CPs), namely {[Mn(4-bpdh)(nip)(H₂O)₂]}_n (1), {[Fe(4-bpdh)(nip)(H₂O)₂]}_n (2), {[Co(4-bpdh)(nip)(H₂O)₂]}_n (3), {[Mn₂(bpp)₂(nip)₂(H₂O)₂]}_n (4), {[Fe(bpp)(nip)(H₂O)]_n (5), [Zn(bpp)(nip)(H₂O)]_n (6), {[Fe(4-bpdh)_{1.5}(nip)]_n·(4-bpdb)_{0.5}}_n (7) and {[Fe(4-bpdb)(nip)]_n·(4-bpdb)_{0.5}(H₂O)]_n (8) using the slow diffusion technique at room temperature. The complexes 1–8 were characterized by single crystal X-ray diffraction analysis and were further characterized by elemental analysis, infrared spectroscopy (IR) and powder X-ray diffraction (PXRD). Complexes 1–3 are isostructural and exhibit a one-dimensional (1D) metal-carboxylate chain with pendant 4-bpdh ligands, which is further extended into a three-dimensional supramolecular structure by means of H-bonding and π - π interactions. Complexes 4–6 are also isomorphous, but distinctly different from the first three complexes. They exhibit a similar 2-fold interpenetrated three-dimensional (3D) net with 6⁶ dia net topology. Compound 7 displays a two-dimensional (2D) grid-like structure, having 4-bpdh ligands in the crystal void, and this is further extended by means of intermolecular π - π interactions into a 3D supramolecular structure, whereas compound 8 possesses a different 2D grid structure containing free 4-bpdb ligands in the void spaces. The thermal stabilities and UV–Vis spectra of all the complexes and the luminescent properties of complex 6 were also studied.

© 2015 Elsevier Ltd. All rights reserved.

1. Introduction

The strategic design of metal organic frameworks (MOFs), also known as coordination polymers (CPs), has received immense interest due to their well controllable network structures [1–5], topological aspects [6,7] and their promising widespread applications as functional materials for the purpose of gas storage and separation [8–11], catalysis [12–14], magnetism [15–17], luminescence [18–21] etc. It has been well established that the design of coordination polymers depends on many factors, such as the nature of the organic ligands and the presence of functional groups [22,23], coordination number of the metal ions [24,25], solvent systems [26–28], pH of the medium [29–31], reaction temperature [32,33], and so on. A precise correlation of the aforesaid factors, however, is yet to be achieved during the crystallization of CPs. It

is needless to mention the importance of crystal structures in discussions on CPs and it is a very common phenomena in the design of CPs, that despite of having all the prerequisites for the reaction, crystals are not afforded at all, or crystals of undesired product are obtained. This indicates that not only the chemical binding but also the ease of crystallization is very crucial in the design of CPs to get a meaningful outcome. Sometimes steric and electronic factors individually or additively facilitate the process of crystallization of CPs and that could also be a very important precondition for the design of CPs.

Based on that, we have picked up a popular isophthalate functionalized ligand with a reasonably bulky and electron withdrawing $-\text{NO}_2$ group at the 5 position. Here, 5-nitroisophthalate (nip^{2-}) possesses the same aromatic skeleton as that of isophthalate (ip^{2-}), along with the uncoordinated 5-position substituent which can exerts a steric effect. That additional steric effect may result in close packing of the structure of CPs and hence facilitate the process of crystallization, offering a new opportunity for the

* Corresponding author.

E-mail address: dghoshal@chemistry.jdvu.ac.in (D. Ghoshal).

discovery of intriguing topologies [34–36]. On the other hand, although the nitro group ($-\text{NO}_2$) in carboxylate ligands does not take part in coordination to transition metal ions, it has a marked impact on the electron density of the whole ligand due to the pulling of electrons by the nitro group from the $-\text{COO}^-$ group present in the 5-nitroisophthalate (nip^{2-}) ring. This reduced electron density may restrict the very common bis-chelating coordination mode of this ligand, making this much more useful for creating structural diversity in comparison to the unsubstituted isophthalate ligand.

As one of the crucial exoteric factors, $\text{N,N}'$ -donor auxiliary linkers are widely used along with polycarboxylate ligands for the design of CPs and careful choice of the $\text{N,N}'$ -donor linker is one of the significant aspects in such synthesis [37–39]. This is basically due to the fact that the conformational rigidity, configurations and substituents on the $\text{N,N}'$ -donor linkers have important roles in controlling the structural assemblies, which further affect the overall network, dimensionality and even the properties of the CPs. In order to investigate the influence of $\text{N,N}'$ -donor co-ligands on the variation of entangled networks and to achieve unusual topologies or physical properties, three different $\text{N,N}'$ -donor linkers with rationally tuned length and rigidity, namely 2,5-bis-(4-pyridyl)-3,4-diaza-2,4-hexadiene (4-bpdh), 1,3-bis-(4-pyridyl)propane (bpp) and 1,4-bis(4-pyridyl)-2,3-diaza-1,3-butadiene (4-bpdb), were introduced into the $\text{M}(\text{nip})$ system (Scheme 1). In this paper, we report the syntheses and structures of eight coordination polymers, namely $\{[\text{Mn}(4\text{-bpdh})(\text{nip})(\text{H}_2\text{O})_2]\cdot\text{H}_2\text{O}\}_n$ (**1**), $\{[\text{Fe}(4\text{-bpdh})(\text{nip})(\text{H}_2\text{O})_2]\cdot\text{H}_2\text{O}\}_n$ (**2**), $\{[\text{Co}(4\text{-bpdh})(\text{nip})(\text{H}_2\text{O})_2]\cdot\text{H}_2\text{O}\}_n$ (**3**), $\{[\text{Mn}_2(\text{bpp})(\text{nip})_2(\text{H}_2\text{O})_2]\cdot\text{H}_2\text{O}\}_n$ (**4**), $\{[\text{Fe}(\text{bpp})(\text{nip})(\text{H}_2\text{O})]\cdot\text{H}_2\text{O}\}_n$ (**5**), $\{[\text{Zn}(\text{bpp})(\text{nip})(\text{H}_2\text{O})]\}_n$ (**6**), $\{[\text{Fe}(4\text{-bpdh})_{1.5}(\text{nip})]\cdot(4\text{-bpdh})_{0.5}\}_n$ (**7**) and $\{[\text{Fe}(4\text{-bpdb})(\text{nip})]\cdot(4\text{-bpdb})_{0.5}(\text{H}_2\text{O})\}_n$ (**8**). All the complexes were characterized by single crystal X-ray crystallography, IR spectroscopy, powder X-ray diffraction (PXRD), elemental analysis, thermogravimetric (TG) analysis and solid state UV–Vis spectroscopy. Moreover, luminescent properties of compound **6** and the bpp ligand were also investigated in detail.

2. Experimental

2.1. Materials

2,5-Bis-(4-pyridyl)-3,4-diaza-2,4-hexadiene (4-bpdh) and 1,4-bis-(4-pyridyl)-2,3-diaza-1,3-butadiene (4-bpdb) were prepared according to literature procedures [40]. The starting materials

4-acetyl pyridine, 4-pyridine carboxaldehyde and hydrazine hydrate for the above synthesis were purchased from Sigma–Aldrich Chemical Co. Inc. and used as received. Highly pure 1,3-bis-(4-pyridyl)propane (bpp), manganese(II) chloride tetrahydrate, iron(II) perchlorate hydrate, cobalt(II) nitrate hexahydrate, zinc(II) nitrate hexahydrate and 5-nitroisophthalic acid (H_2nip) were purchased from Sigma–Aldrich Chemical Co. Inc. and used as received. The sodium salt of 5-nitroisophthalic acid (Na_2nip) was synthesized by the gradual addition of Na_2CO_3 to a H_2nip water suspension in a 1:1 ratio. The neutralization was checked by measuring the pH of the solution and then it was allowed to stand for 8 h. Finally the solvent was evaporated using a water bath until dry. All other chemicals and solvents were AR grade and were used as received.

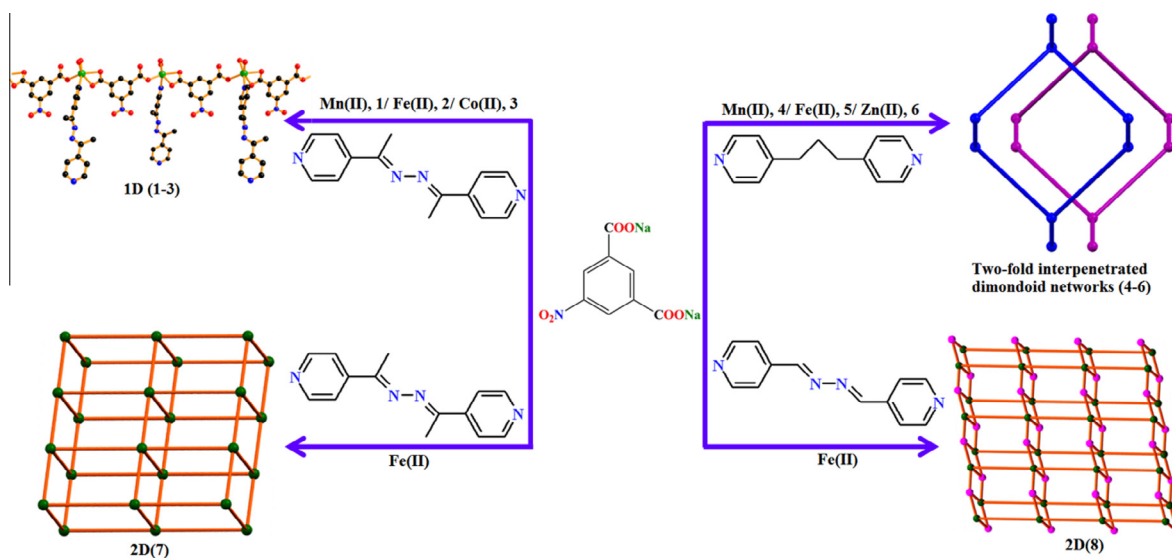
2.2. Physical measurements

Elemental analyses (carbon, hydrogen and nitrogen) were performed using a Heraeus CHNS analyzer. Infrared spectra ($4000\text{--}400\text{ cm}^{-1}$) were taken on KBr pellets, using a PerkinElmer Spectrum BX-II IR spectrometer. X-ray powder diffraction (PXRD) patterns of the bulk samples were recorded in a Bruker D8 Discover instrument using $\text{Cu K}\alpha$ radiation. Thermal analysis (TGA) was carried out on a METTLER TOLEDO TGA 850 thermal analyzer under a nitrogen atmosphere (flow rate: $50\text{ cm}^3\text{ min}^{-1}$), in the temperature range $30\text{--}600\text{ }^\circ\text{C}$ with a heating rate of $2\text{ }^\circ\text{C min}^{-1}$. UV–Vis spectra were recorded on a Perkin Elmer Lambda 35 UV–Vis spectrophotometer. Emission spectra were recorded on a HORIBA Jobin Yvon (Fluoromax-3) fluorescence spectrophotometer.

2.3. Syntheses

2.3.1. $\{[\text{Mn}(4\text{-bpdh})(\text{nip})(\text{H}_2\text{O})_2]\cdot\text{H}_2\text{O}\}_n$ (**1**)

An aqueous solution (20 mL) of Na_2nip (1 mmol, 0.255 g) was mixed with a methanolic solution (20 mL) of 2,5-bis-(4-pyridyl)-3,4-diaza-2,4-hexadiene (4-bpdh) (1 mmol, 0.238 g) and stirred for 30 min to mix it well. $\text{MnCl}_2\cdot 4\text{H}_2\text{O}$ (1 mmol, 0.198 g) was dissolved in 20 mL of water in a separate beaker. In a crystal tube, 3 ml of the Mn(II) solution was then slowly and carefully layered with 6 ml of above mentioned mixed-ligand solution using 3 ml of buffer solution (1:1 of H_2O and MeOH) between the two solutions. The tube was sealed and kept undisturbed at room temperature and after seven days colorless block shaped single crystals suitable for X-ray diffraction analysis were obtained at the wall



Scheme 1. Synthetic outline for complexes 1–8.

of the tube. The crystals were separated and washed with a methanol–water (1:1) mixture and dried under air (Yield: 63%). *Anal. Calc.* for $C_{22}H_{23}N_5O_9$ Mn: C, 47.49; H, 4.17; N, 12.59. Found: C, 47.51; H, 4.22; N, 12.55%. IR spectra (cm^{-1}): $\nu(H_2O)$ 3403; $\nu(C=N)$ 1602; $\nu(N=O)$ 1543(as), 1376(s); $\nu(C-O)$ 1293–1221; $\nu(CH-Ar)$ 3097; $\nu(C=C)$ 1606–1422.

2.3.2. $\{[Fe(4-bpdh)(nip)(H_2O)_2] \cdot H_2O\}_n$ (**2**) and $\{[Fe(4-bpdh)_{1.5}(nip)](4-bpdh)_{0.5}\}_n$ (**7**)

These two compounds were identified simultaneously by following the same procedure as that for **1**, but using $Fe(ClO_4)_2 \cdot xH_2O$ (1 mmol, 0.255 g) instead of $MnCl_2 \cdot 4H_2O$ in the single layer reaction. The yield of yellowish block shaped single crystals of compound **2** was greater than the reddish block shaped crystals of compound **7**. Both the single crystals of **2** and **7**, suitable for X-ray diffraction analysis, were obtained after 15 days. The crystals were separated manually and washed with a methanol–water (1:1) mixture and dried under air. For **2** (Yield: 45%) *Anal. Calc.* for $C_{22}H_{23}N_5O_9Fe$: C, 47.41; H, 4.16; N, 12.57. Found: C, 47.48; H, 4.2; N, 12.53%. IR spectra (cm^{-1}): $\nu(H_2O)$ 3395; $\nu(C=N)$ 1607; $\nu(N=O)$ 1554(as), 1378(s); $\nu(C-O)$ 1298–1211; $\nu(CH-Ar)$ 3101–3041; $\nu(C=C)$ 1604–1416. For **7** (Yield 22%) *Anal. Calc.* for $C_{36}H_{31}N_9O_6Fe$: C, 58.31; H, 4.21; N, 17. Found: C, 58.39; H, 4.25; N, 17.4%. IR spectra (cm^{-1}): $\nu(C=N)$ 1610; $\nu(N=O)$ 1528(as), 1362(s); $\nu(C-O)$ 1289–1216; $\nu(CH-Ar)$ 3076; $\nu(C=C)$ 1528–1413.

2.3.3. $\{[Co(4-bpdh)(nip)(H_2O)_2] \cdot H_2O\}_n$ (**3**)

This compound was synthesized by following the same procedure as that used for **1**, but with $Co(NO_3)_2 \cdot 6H_2O$ (1 mmol, 0.297 g) instead of $MnCl_2 \cdot 4H_2O$. Pink colored block shaped single crystals suitable for X-ray diffraction analysis were obtained after two weeks. The crystals were separated and washed with a methanol–water (1:1) mixture and dried under air (yield: 62%). *Anal. Calc.* for $C_{22}H_{23}N_5O_9Co$: C, 47.15; H, 4.14; N, 12.5. Found: C, 47.23; H, 4.19; N, 12.54%. IR spectra (cm^{-1}): $\nu(H_2O)$ 3420; $\nu(C=N)$ 1607; $\nu(N=O)$ 1535–1556(as), 1350(s); $\nu(C-O)$ 1292–1219; $\nu(CH-Ar)$ 3102; $\nu(C=C)$ 1610–1416.

2.3.4. $\{[Mn_2(bpp)_2(nip)_2(H_2O)_2] \cdot H_2O\}_n$ (**4**)

This was synthesized by the same procedure as that used for **1**, but with 1,3-bis-(4-pyridyl)propane (bpp) (1 mmol, 0.198 g) instead of 2,5-bis-(4-pyridyl)-3,4-diaza-2,4-hexadiene (4-bpdh) (1 mmol, 0.238 g). Colorless block shaped crystals suitable for X-ray diffraction analysis were obtained after seven days. The crystals were separated and washed with a methanol–water (1:1) mixture and dried under air (Yield 70%). *Anal. Calc.* for $C_{42}H_{40}N_6O_{15}Mn_2$: C, 51.55; H, 4.12; N, 8.59. Found: C, 51.59; H, 4.16; N, 8.54%. IR spectra (in cm^{-1}): $\nu(H_2O)$ 3399; $\nu(C=N)$ 1622; $\nu(N=O)$ 1530(as), 1359(s); $\nu(C-O)$ 1222; $\nu(CH-Ar)$ 3102; $\nu(C=C)$ 1530–1426.

2.3.5. $\{[Fe(bpp)(nip)(H_2O)] \cdot H_2O\}_n$ (**5**)

This has been synthesized by the same procedure as that used for **4**, but with $Fe(ClO_4)_2 \cdot xH_2O$ (1 mmol, 0.255 g) instead of $MnCl_2 \cdot 6H_2O$. Reddish block shaped crystals suitable for X-ray diffraction analysis were obtained after seven days. The crystals were separated and washed with a methanol–water (1:1) mixture and dried under air (Yield 65%). *Anal. Calc.* for $C_{21}H_{21}N_3O_8Fe$: C, 50.52; H, 4.24; N, 8.42. Found: C, 50.55; H, 4.28; N, 8.4%. IR spectra (cm^{-1}): $\nu(H_2O)$ 3398; $\nu(C=N)$ 1633; $\nu(N=O)$ 1535(as), 1367(s); $\nu(C-O)$ 1221; $\nu(CH-Ar)$ 3099; $\nu(C=C)$ 1539–1425.

2.3.6. $[Zn(bpp)(nip)(H_2O)]_n$ (**6**)

This has been synthesized by the same procedure as that used for **4**, but with $Zn(NO_3)_2 \cdot 6H_2O$ (1 mmol, 0.297 g) instead of $MnCl_2 \cdot 4H_2O$ (1 mmol, 0.198 g). Colorless block shaped crystals

suitable for X-ray diffraction analyses were obtained after 10 days. The crystals were separated and washed with a methanol–water (1:1) mixture and dried under air (Yield 55%). *Anal. Calc.* for $C_{21}H_{19}N_3O_7Zn$: C, 51.39; H, 3.9; N, 8.56. Found: C, 51.41; H, 3.14; N, 8.51%. IR spectra (cm^{-1}): $\nu(H_2O)$ 3437; $\nu(C=N)$ 1640; $\nu(N=O)$ 1526(as), 1360(s); $\nu(C-O)$ 1226; $\nu(CH-Ar)$ 3104; $\nu(C=C)$ 1530.

2.3.7. $\{[Fe(4-bpdb)(nip)](4-bpdb)_{0.5}(H_2O)\}_n$ (**8**)

This product was synthesized by the same procedure as that used for **2**, but with 4-bpdb (1 mmol, 0.210 g) instead of 4-bpdh (1 mmol, 0.238 g). Deep red colored block shaped crystals suitable for X-ray diffraction analysis were obtained after ten days. The crystals were separated and washed with a methanol–water (1:1) mixture and dried under air (Yield 70%). *Anal. Calc.* for $C_{26}H_{20}N_7O_7Fe$: C, 52.19; H, 3.37; N, 16.39. Found: C, 52.24; H, 3.34; N, 16.44%. IR spectra (cm^{-1}): $\nu(H_2O)$ 3461; $\nu(C=N)$ 1632; $\nu(N=O)$ 1528(as), 1383(s); $\nu(C-O)$ 1237; $\nu(CH-Ar)$ 3086; $\nu(C=C)$ 1538.

The bulk compounds of six complexes, except **2** and **7**, were synthesized in the powder form by the direct mixing of the corresponding ligand solutions and the M(II) salt solution in water in an equal-molar ratio. In the case of **2** and **7**, the bulk products were prepared as crystals, following the procedure mentioned in Section 2.3.2. The purity of the complexes was verified by PXRD, which gave a good correspondence between the simulated PXRD patterns. The purity of the bulk sample was further confirmed by the results of elemental analysis and IR spectra as well, which were also found to be in accordance with the data obtained for the single crystals.

2.4. Crystallographic data collection and refinement

Suitable single crystals of compounds **1–8** were mounted on the tip of thin glass fibers with commercially available super glue. X-ray single crystal data collection of all eight crystals were performed at room temperature using a Bruker APEX II diffractometer, equipped with a normal focus, sealed tube X-ray source with graphite monochromated Mo $K\alpha$ radiation ($\lambda = 0.71073 \text{ \AA}$). The data were integrated using the SAINT [41] program and the absorption corrections were made with SADABS [42]. All the structures were solved by SHELXS 97 [43] using the Patterson method and followed by successive Fourier and difference Fourier synthesis. Full matrix least-squares refinements were performed on F^2 using SHELXL-97 [43] with anisotropic displacement parameters for all non-hydrogen atoms. All the hydrogen atoms were fixed geometrically by the HFIX command and placed in ideal positions in the case of all structures except **3**, where the hydrogen atoms of water molecules were located from the Fourier map. The thermal parameter of the O atom of the lattice water is quite high for **4** and **5**, thus the H-atom of the said O atom could not be located properly. Additionally in case of **4**, one of the H atoms of the coordinated water molecule O1W has been found with a two fold disorder and thus has been fixed with occupancies at 0.5. All calculations were carried out using SHELXS 97, SHELXL 97, PLATON v1.15 [44], ORTEP-3v2 [45] and WINGX system Ver-1.80 [46] and TOPOS [47,48]. Data collection and structure refinement parameters and crystallographic data for all the complexes are given in Table 1.

3. Results and discussion

3.1. Crystal structure descriptions of the CPs

The structural diversity of the eight CPs are depicted in Scheme 1, exhibiting various coordination modes of the nip^{2-} dianion (Scheme 2) and structural differences of the linear dipyridyl

Table 1
Crystallographic and structural refinement parameters of complexes **1–8**.

	1	2	3	4
Formula	C ₂₂ H ₂₃ N ₅ O ₉ Mn	C ₂₂ H ₂₃ N ₅ O ₉ Fe	C ₂₂ H ₂₃ N ₅ O ₉ Co	C ₄₂ H ₄₀ N ₆ O ₁₅ Mn ₂
Formula weight	556.39	557.30	560.38	978.68
Crystal system	monoclinic	monoclinic	monoclinic	orthorhombic
Space group	<i>P21/c</i>	<i>P21/c</i>	<i>P21/c</i>	<i>Pnna</i>
<i>a</i> (Å)	16.4823(3)	16.419(5)	16.3446(2)	17.2254(4)
<i>b</i> (Å)	7.5363(2)	7.505(5)	7.5226(1)	14.0118(3)
<i>c</i> (Å)	19.7751(4)	19.650(5)	19.5825(3)	18.2207(5)
α (°)	90	90	90	90
β (°)	91.101(1)	91.254(5)	90.976(1)	90
γ (°)	90	90	90	90
<i>V</i> (Å ³)	2455.92(9)	2420.8(19)	2407.40(6)	4397.73(18)
<i>Z</i>	4	4	4	4
<i>D_c</i> (g cm ⁻³)	1.505	1.529	1.546	1.475
μ (mm ⁻¹)	0.599	0.685	0.776	0.651
<i>F</i> (000)	1148	1152	1156	2008
θ range (°)	1.2–27.5	1.2–27.6	2.1–27.5	1.6–27.5
Reflections collected	38368	39541	37267	68034
Unique reflections	5640	5558	5517	5076
Reflections <i>I</i> > 2 σ (<i>I</i>)	4655	4351	4478	3749
<i>R</i> _{int}	0.030	0.037	0.040	0.035
Goodness-of-fit (<i>F</i> ²)	1.07	1.01	1.03	1.03
<i>R</i> ₁ (<i>I</i> > 2 σ (<i>I</i>)) ^a	0.0344	0.0369	0.0313	0.0446
<i>wR</i> ₂ (<i>I</i> > 2 σ (<i>I</i>)) ^a	0.1131	0.1126	0.0848	0.1406
$\Delta\rho$ min/max (e Å ³)	–0.41, 0.45	–0.42, 0.33	–0.34, 0.35	–0.44, 0.72
	5	6	7	8
Formula	C ₂₁ H ₂₁ N ₃ O ₈ Fe	C ₂₁ H ₁₉ N ₃ O ₇ Zn	C ₃₆ H ₃₁ N ₉ O ₆ Fe	C ₂₆ H ₂₀ N ₇ O ₇ Fe
Formula weight	499.26	490.78	741.55	598.34
Crystal system	orthorhombic	monoclinic	triclinic	triclinic
Space group	<i>Pnna</i>	<i>C2/c</i>	<i>P</i> $\bar{1}$	<i>P</i> $\bar{1}$
<i>a</i> (Å)	17.1017(5)	14.322(5)	10.072(5)	10.0749(6)
<i>b</i> (Å)	14.0287(4)	18.378(5)	12.349(5)	10.1223(5)
<i>c</i> (Å)	18.1303(5)	16.194(5)	15.655(5)	14.1708(9)
α (°)	90	90	108.615(5)	85.611(4)
β (°)	90	100.945(5)	95.044(5)	78.733(4)
γ (°)	90	90	108.650(5)	74.380(4)
<i>V</i> (Å ³)	4349.7(2)	4185(2)	1708.8(12)	1364.52(14)
<i>Z</i>	8	8	2	2
<i>D_c</i> (g cm ⁻³)	1.519	1.558	1.441	1.456
μ (mm ⁻¹)	0.747	1.223	0.503	0.611
<i>F</i> (000)	2048	2016	768	614
θ range (°)	1.6–27.5	1.8–27.6	1.4–27.6	1.5–27.6
Reflections collected	68693	33489	27850	38470
Unique reflections	5024	4836	7765	6052
Reflections <i>I</i> > 2 σ (<i>I</i>)	3843	2561	4781	3046
<i>R</i> _{int}	0.033	0.126	0.049	0.094
Goodness-of-fit (<i>F</i> ²)	1.03	0.99	1.02	1.10
<i>R</i> ₁ (<i>I</i> > 2 σ (<i>I</i>)) ^a	0.0366	0.0619	0.0671	0.1291
<i>wR</i> ₂ (<i>I</i> > 2 σ (<i>I</i>)) ^a	0.1136	0.1682	0.1957	0.2807
$\Delta\rho$ min/max (e Å ³)	–0.41 0.45	–0.61, 0.46	–0.40, 0.93	–0.75, 0.81

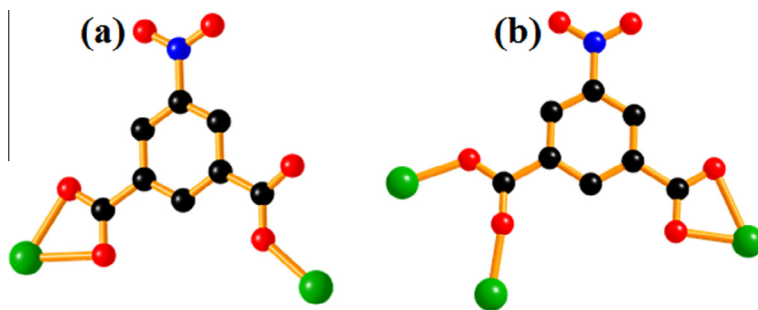
$$^a R_1 = \sum ||F_o| - |F_c|| / \sum |F_o|, wR_2 = [\sum (w(F_o^2 - F_c^2)^2) / \sum w(F_o^2)^2]^{1/2}.$$

linkers in complexes **1–8**. Moreover, structural details for all the complexes are discussed below.

3.1.1. $\{[M(4\text{-bpdh})(\text{nip})(\text{H}_2\text{O})_2]\cdot\text{H}_2\text{O}\}_n$ [*M* = Mn for **1**, Fe for **2** and Co for **3**]

Single-crystal X-ray structural analysis revealed that compounds **1–3** are isostructural, having the monoclinic *P21/c* space group with a *Z* value of 4. All the compounds show the formation of a one-dimensional (1D) structure of M(II) [*M* = Mn for **1**, Fe for **2** and Co for **3**] ions linked by the 5-nitroisophthalate dianion (nip²⁻) in a bridging chelate-monodentate fashion, where the 4-bpdh ligand is pendent. The asymmetric unit of all three compounds contains one M(II) ion, one 4-bpdh ligand, one 5-nitroisophthalate ligand, two coordinated water and one lattice water molecule. The M(II) ion shows a distorted octahedral geometry with MO₅N coordination environment (Fig. 1a for **1**, S1a for **2** and S2a for **3**). Here, each metal center is ligated to three oxygen

atoms (O1, O5^a and O6^a) of two different nip²⁻ ligands, two coordinated water molecules (O1W and O2W) and one pyridyl nitrogen atom (N1) of a 4-bpdh linker. In compounds **1–3**, the M(II)–O bond lengths vary from 2.1092(14) to 2.2697(12) Å (Mn–O for **1**), 2.038(3) to 2.259(2) Å (Fe–O for **2**) and 2.0329(12) to 2.1554(13) Å (Co–O for **3**), and the corresponding M(II)–N bond lengths for **1–3** are 2.3177(15) Å (Mn–N for **1**), 2.392(2) Å (Fe–N for **2**) and 2.1886(14) Å (Co–N for **3**) (Tables S1–S3). Here, one end of the 5-nitroisophthalate ligand binds in a bridging monodentate fashion and the other end binds in a chelating fashion between two metal centers, resulting in the formation of a 1D metal carboxylate chain (Fig. 1b for **1**, S1b for **2** and S2b for **3**) along the *c*-axis. In the crystal packing, the coordinated water molecules and the lattice water molecule are attached to each other, along with the carboxylate oxygen atoms of the 5-nitroisophthalate ligand, and one coordinated water molecule is also attached to the pyridyl N-atom by means of H-bonding forming a 2D sheet in the



Scheme 2. Different bridging modes of 5-nitroisophthalate (nip^{2-}); (a) chelating-monodentate in **1–7** and (b) chelating-bidentate in **8**.

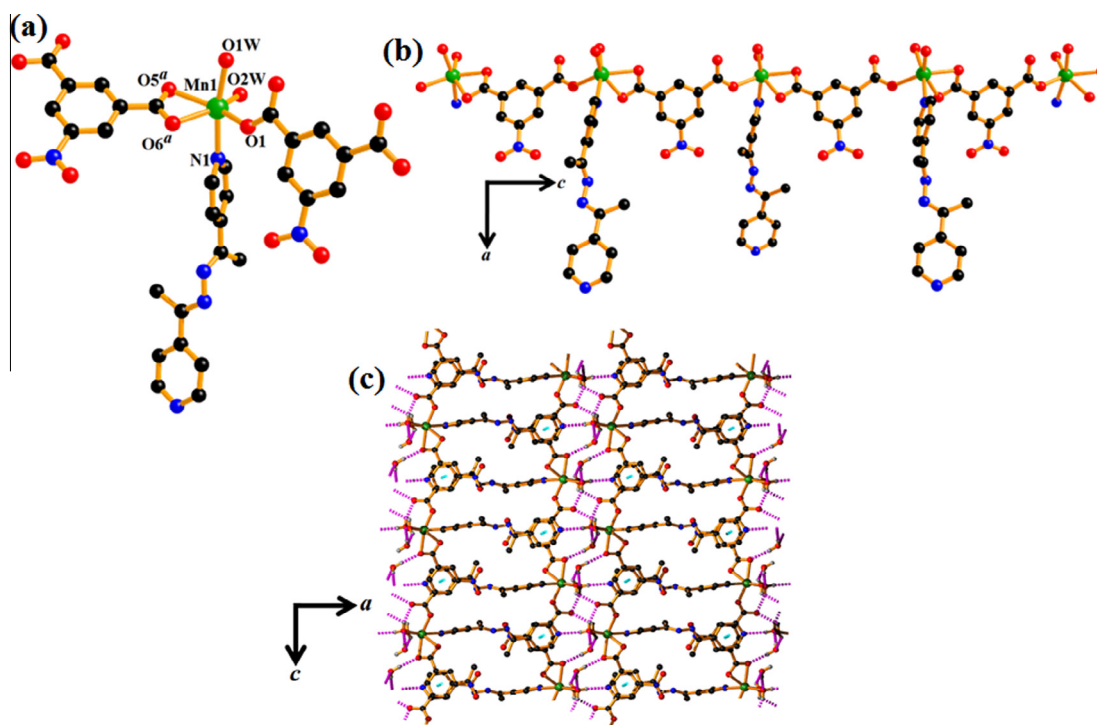


Fig. 1. (a) Coordination environment around the Mn(II) ions in **1**; Mn (green), N (blue), O (red), C (black). (b) 1D metal carboxylate chain with pendant 4-bpdh ligands in **1**. (c) Supramolecular 3D structures in **1** by locking 1D chains through π - π interactions and H-bonding (π - π interactions: cyan dotted lines and H-bonding: pink dotted lines). (Color online.)

crystallographic ac plane in all three cases (Table S4). These 2D sheets are further stitched through intermolecular π - π interactions (Table S5) with the help of pendent 4-bpdh ligands, resulting in a supramolecular three-dimensional (3D) structure (Fig. 1c for **1**, S1c for **2** and S2c for **3**).

3.1.2. $\{[\text{Mn}_2(\text{bpp})_2(\text{nip})_2(\text{H}_2\text{O})_2] \cdot \text{H}_2\text{O}\}_n$ (**4**), $\{[\text{Fe}(\text{bpp})(\text{nip})(\text{H}_2\text{O})] \cdot \text{H}_2\text{O}\}_n$ (**5**) and $[\text{Zn}(\text{bpp})(\text{nip})(\text{H}_2\text{O})]_n$ (**6**)

Single-crystal structural analysis revealed that **4** and **5** are isostructural, whereas in **6** the coordination structure is similar to that of **4/5**, but with a minor difference with respect to the lattice water molecule. Compounds **4** and **5** crystallize in the orthorhombic $Pnna$ space group with $Z=4$ and 8, respectively, whereas compound **6** crystallizes in the monoclinic $C2/c$ space group with a Z value of 8.

Structural analysis of compounds **4** and **5** reveal the formation of a three-dimensional (3D) structure of $\text{M(II)} [M = \text{Mn}$ for **4** and Fe for **5**] ions linked by 5-nitroisophthalate dianions (nip^{2-}) in the bridging chelate-monodentate fashion and a bridging bpp ligand. The asymmetric unit of both **4** and **5** contains one M(II) ion, one bpp

ligand, one 5-nitroisophthalate ligand, one coordinated water and one lattice water molecule, exhibiting a distorted octahedral geometry with MO_4N_2 coordination environment (Fig. 2a for **4** and S4a for **5**). Each metal ion is connected to three oxygen atoms (O1 , O5^b and O6^b) of two different bridging nip^{2-} ligands, one coordinated water molecule (O1W) and two pyridyl nitrogen atoms (N1 and N2^a) of 4-bpp linkers. In compounds **4** and **5**, the $\text{M(II)}-\text{O}$ bond length varies from 2.0970(18) to 2.3519(16) Å ($\text{Mn}-\text{O}$ for **4**) and 2.0305(15) to 2.3769(16) Å ($\text{Fe}-\text{O}$ for **5**), respectively, and the corresponding $\text{M(II)}-\text{N}$ bond lengths for **4** and **5** are 2.2317(18) to 2.287(2) Å ($\text{Mn}-\text{N}$ for **4**) and 2.1624(16) to 2.2173(18) Å ($\text{Fe}-\text{N}$ for **5**) (Tables S6 and S7). The bridging nip^{2-} ligand is bonded to two metal ions in a chelate-monodentate fashion and extends the structure along the a -axis (Fig. S3a for **4** and S5a for **5**), whereas the bridging bpp ligand also connects two metal centers. Here six nip^{2-} and six bpp ligands linked with the M(II) centres form an adamantoid cage structure (Fig. 2b and c, S3b for **4** and S4b, S4c, S5b for **5**). These adamantoid cages are interlinked to form a three dimensional diamondoid structure (Fig. 2d, S3c for **4** and S4d, S5c for **5**). The $\text{M} \cdots \text{M}$ separation through the nip^{2-} and bpp ligands are 8.998

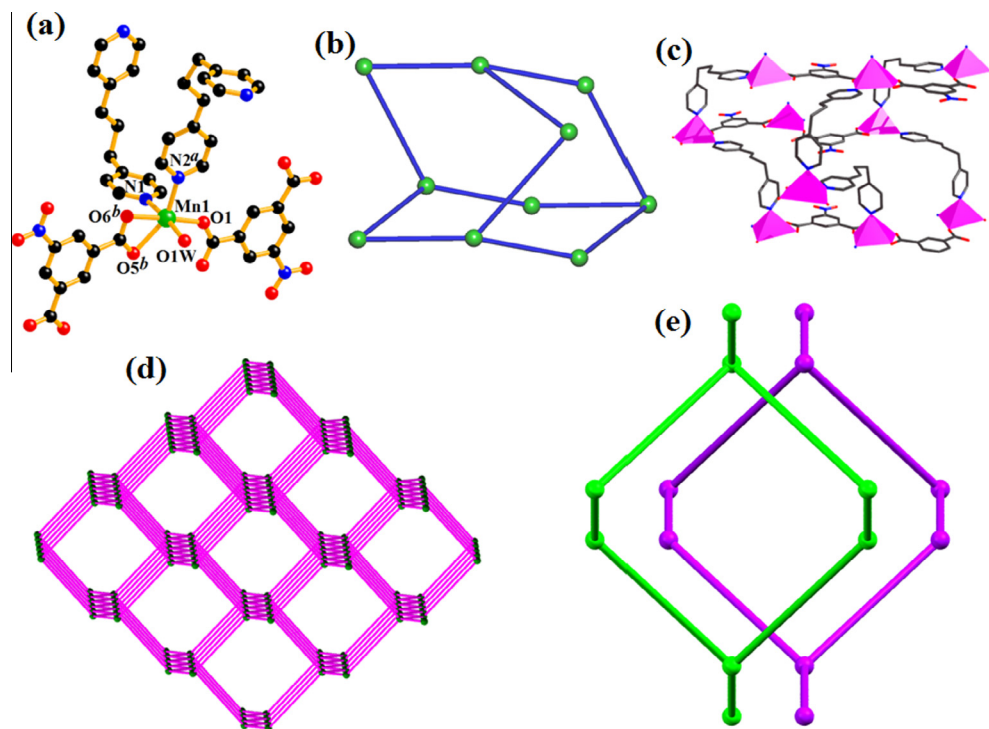


Fig. 2. (a) Coordination environment around the Mn(II) ions in **4**; Mn (green), N (blue), O (red), C (black). (b,c) Wire frame model and polyhedral presentation of a single adamantoid cage constructed through six bpp and six 5-nitroisophthalate ligands bridging with the Mn(II) centers in **4**, respectively. (d) A single 4-connected 3D-diamondoid network in **4**. (e) Topological representation of the 2-fold interpenetrating diamondoid networks in **4**. (Color online.)

and 11.350 Å (Mn···Mn for **4**) and 8.936 and 11.302 Å (Fe···Fe for **5**), respectively. Due to this spacious nature of the diamondoid cavities, in both the structures, two equivalent complementary diamondoid networks interpenetrate each other to exhibit an overall 2-fold interpenetrated diamondoid network (Fig. 2e for **4** and S4e for **5**). Moreover, notable π - π stacking further stabilizes the interpenetrating diamondoid networks (Table S5). Topological analysis of **4** and **5** with TOPOS [47,48] suggests that each M(II) center acts as a 4-connecting uninodal node (Figs. 2d and S4d), and the overall structure has a 6⁶-*dia* net topology. The interpenetration analysis also [47,48] suggests the presence of Class IIa interpenetration with $Z_t = 1$ and $Z_n = 2$.

[Zn(bpp)(nip)(H₂O)]_n (**6**) also had a similar type of diamondoid structure as that of **4** and **5**, only differing with respect to the lattice water molecule. In **6** the bpp ligand shows more flexibility than in **4** and **5**, as a result the adamantoid cages formed here are squeezed in comparison to those of **4** and **5**. This results in the squeezing of the diamondoid network and probably the change of the space group to lower symmetry (orthorhombic *Pnna* to monoclinic *C2/c*). This squeezing may also account for the absence of lattice water molecules in the crystal structure of **6**. The relevant tables and figures related to the structure of **6** are reported in the ESI (Figs. S6–S7; Table 1, S8 and S5).

3.1.3. {[Fe(4-bpdb)_{1.5}(nip)]·(4-bpdb)_{0.5}}]_n (**7**)

Compound **7** crystallizes in the triclinic *P* $\bar{1}$ space group with a *Z* value of 2. Single-crystal X-ray structure analysis reveals the formation of a two dimensional (2D) sheet structure with Fe(II) metal ions connected by 5-nitroisophthalate and 4-bpdb linkers. The asymmetric unit of **7** contains one Fe(II) ion, one and half bridging 4-bpdb ligands, one 5-nitroisophthalate ligand and half a lattice 4-bpdb ligand. The central Fe(II) ion (Fe1) adopts a distorted octahedral geometry surrounded by three oxygen atoms (O1, O2 and O6^a) from two different nip²⁻ ligands and three nitrogen atoms (N1, N5

and N4^b) from three different 4-bpdb ligands (Fig. 3a). The Fe–O bond lengths lie in the range 2.007(3)–2.416(3) Å, whereas the Fe–N bond lengths are 2.209(3)–2.241(3) Å (Table S9). Here, the nip²⁻ ligand binds in a bridging monodentate-chelate fashion, as found in **1–6**, and forms 1D chains along the *a*-axis; two such parallel chains are connected by 4-bpdb ligands to form a 1D ladder extended along the *a*-axis (Fig. 3b). These 1D ladders are connected through another set of bridging 4-bpdb ligands and extend the structure into a 2D sheet (Fig. 3c and d). There are uncoordinated lattice 4-bpdb ligands situated in the voids of the crystal framework. The overall structure is also stabilized by intermolecular π - π interactions (Fig. S8, Table S10). TOPOS [47,48] analysis reveals that the structure can be represented as a 5-connected uninodal net (Fig. 3e) with a point symbol of {4⁸.6²}.

3.1.4. {[Fe(4-bpdb)(nip)]·(4-bpdb)_{0.5}(H₂O)]_n (**8**)

Compound **8** crystallizes in the triclinic *P* $\bar{1}$ space group with a *Z* value of 2. The structure analysis revealed the formation of two dimensional (2D) sheets of **8** containing the free 4-bpdb linker in the network void. Here each asymmetric unit of **8** contains one Fe(II) ion, one coordinated bridging 4-bpdb linker, one 5-nitroisophthalate ligand, half a lattice 4-bpdb ligand and one lattice water molecule, forming a distorted octahedral geometry with FeO₄N₂ coordination environment (Fig. 4a). There are one water molecule and half a 4-bpdb molecule in the lattice in each formula unit. Here each of the Fe(II) ions is linked to four oxygen atoms (O1, O2, O5^b and O6^c) of three different nip²⁻ ligands and two nitrogen atoms of two different 4-bpdb linkers (N1 and N4^a). The Fe1–N and Fe1–O distances are 2.182(7)–2.183(8) and 2.045(7)–2.321(7) Å, respectively (Table S11). Here, one end of the nip²⁻ linkers binds in a bridging bidentate fashion and the other end binds in chelating mode linking two metal centers to create one dimensional metal carboxylate ribbons (Fig. 4b) extended along the *b*-axis. These 1D

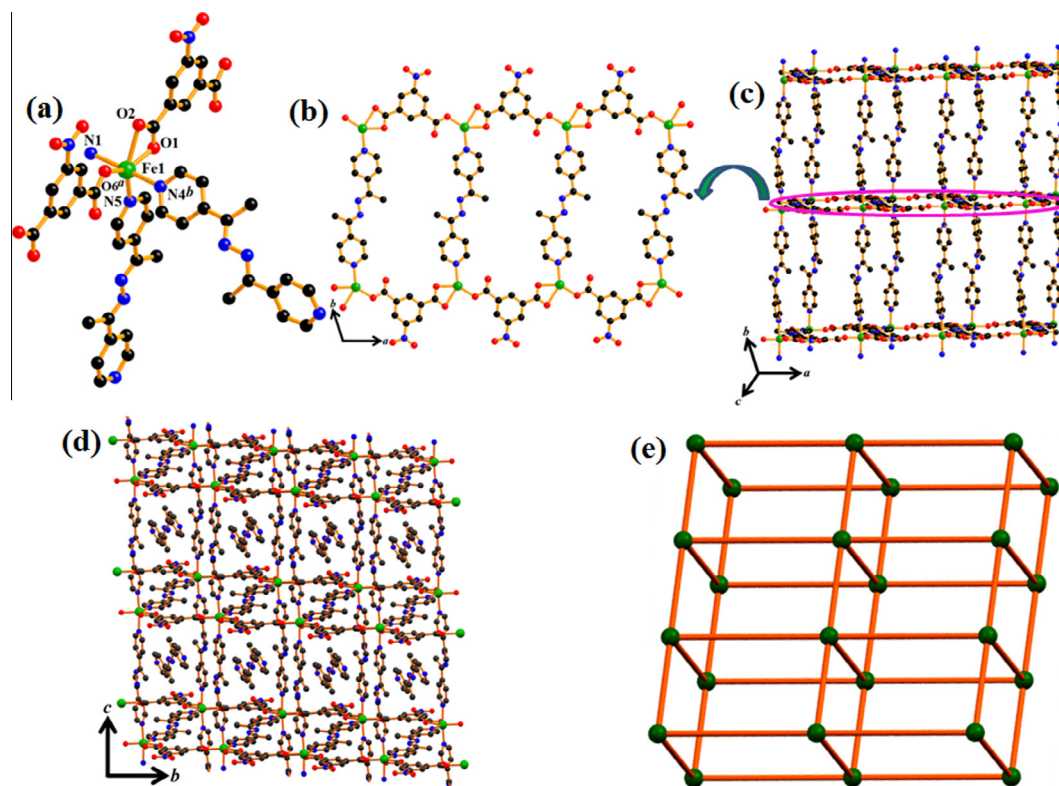


Fig. 3. (a) Coordination environment around the Fe(II) ions in **7**; Fe (green), N (blue), O (red), C (black). (b) View of the 1D ladder in **7**. (c) 2D sheet in **7** constructed by both 5-nitroisophthalate and 4-bpbdh ligands (free 4-bpbdh ligands are omitted for clarity). (d) 2D sheet containing a free 4-bpbdh ligand in the void space of **7**. (e) Topological representation of the 5-connected 2D sheet of **7**. (Color online.)

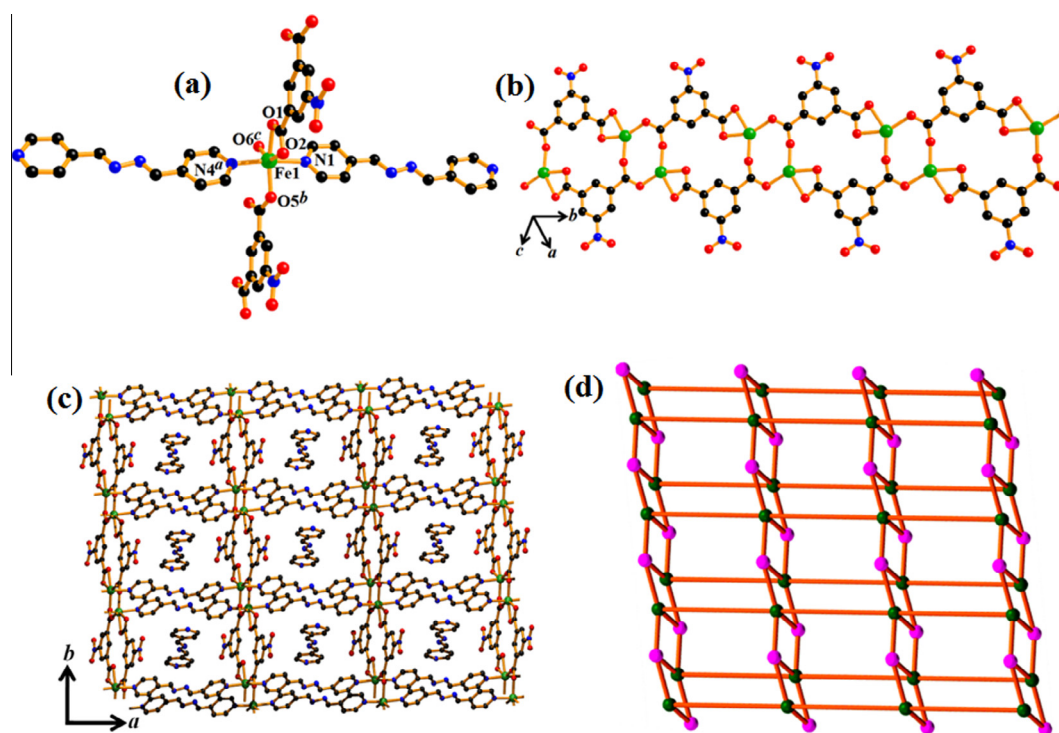


Fig. 4. (a) Coordination environment around the Fe(II) ions in **8**; Fe (green), N (blue), O (red), C (black). (b) 1D metal carboxylate chain in **8** along the *b*-axis (4-bpbdh ligands are omitted for clarity). (c) 2D sheet containing the free 4-bpbdh ligand in the pore in **8** (d) Topological representation of (3,5)-connected binodal 2D sheet in **8**; Fe (green) and Nip^{2-} (pink). (Color online.)

ribbons are further extended into a 2D sheet in the *ab* plane with the linkage of 4-bpdb ligands (Fig. 4c). The 2D sheet contains an uncoordinated lattice 4-bpdb ligand and a lattice water molecule in the cavities of the 2D layer. Network analysis by TOPOS [47,48] suggests that the structure of **8** can be represented as a (3,5)-connected binodal net with stoichiometry (3-c)(5-c) (Fig. 4d) and the corresponding Schläfli symbol is $\{4^2 \cdot 6^7 \cdot 8\}\{4^2 \cdot 6\}$.

3.2. Powder X-ray diffraction (PXRD)

Powder X-ray diffraction (PXRD) analysis was carried out to confirm the phase purity of the bulk materials for all the compounds at room temperature. The experimental PXRD patterns of complexes **1–8** are in good agreement with the simulated ones from their corresponding single crystal structures (Fig. S17–S24), confirming the phase purity of the complexes.

3.3. Thermogravimetric analysis (TGA)

To investigate the thermal stabilities of complexes **1–8**, their thermal behaviours were studied by thermogravimetric analysis (TGA). The TGA experiments were performed on complexes **1–8** in the temperature range 30–600 °C under a N₂ atmosphere at a heating rate of 10 °C min⁻¹. The TGA curves for complexes **1–8** are shown in Fig. S25. The TGA curves of the isostructural complexes **1**, **2** and **3** are very similar, with two continuous weight losses. In each case the first step indicates the loss of a loosely H-bonded guest water molecule in the temperature range ~55–60 °C and the second step for the loss of two strongly H-bonded coordinated water molecules in the temperature range ~130–160 °C. A sharp weight loss in the temperature range ~55–160 °C (found 10.7% for **1**, 9.65% for **2**, 9.5% for **3**) was attributed to the loss of the one lattice and two coordinated water molecules (calcd 9.7% for **1**, 9.7% for **2**, 9.6% for **3**) and the dehydrated frameworks are further stable up to the temperature range ~360–370 °C. After that, they gradually decompose into their corresponding metal oxides nearly at 600 °C. In the case of compounds **4** and **5**, loss of their lattice water molecule occurs at room temperature and the thermogravimetric analysis (TGA) also supports this. The TGA curves of the isostructural compounds **4–6** are also similar, with a single step weight loss. Complexes **4**, **5** and **6** are thermally stable up to 250 °C, with a weight loss in the temperature range 120–160 °C (found 3.44% for **4**, 3.66% for **5**, 3.3% for **6**), corresponding to the release of one coordinated water molecule (calcd 3.74% for **4**, 3.74% for **5**, 3.66% for **6**); after that on further heating they decomposes into their corresponding metal oxides before 600 °C. For **7**, the TGA curve shows no significant weight loss up to 225 °C, due to the absence of any solvent molecules, finally leading to the formation of ferrous oxide at nearly 600 °C. In the case of **8**, the removal of the guest water molecule is observed within the temperature range 80–95 °C (found, 3.1%; calcd, 3.0%), and the decomposition of the compound occurs at 220 °C (Fig. S25) and it finally collapses into ferrous oxide at nearly 560 °C.

3.4. Solid-state absorption spectra

The UV–Vis absorption spectra of complexes **1–8** along with the free N,N'-donor linkers (4-bpdh, bpp and 4-bpdb) were measured in the solid state at room temperature. As shown in Fig. S26, 4-bpdh shows two peaks at 253 and 340 nm in the UV range, which corresponds to the π - π^* or n - π^* transition of the aromatic ring [49,50]. However, complex **1** exhibits an intense peak at 309 nm, which is a different from that of the 4-bpdh linker, indicating that it may be generated from an intraligand transition (ILCT) or metal to ligand charge-transfer transition (MLCT) [49,50]. Complexes **2–3** and **7** show UV absorption with maxima at 315 and 415 nm (for **2**),

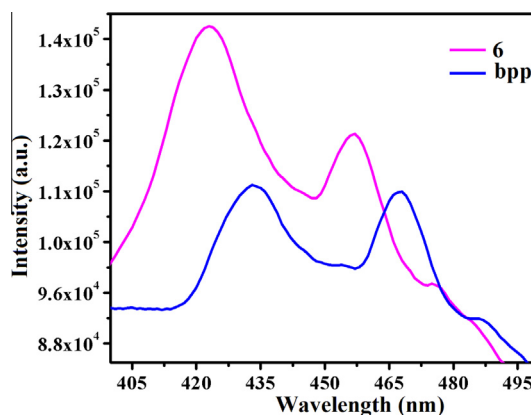


Fig. 5. Emission spectra of complex **6** and the free N,N'-donor linker bpp.

263 and 332 nm (for **3**) and 471 and 612 nm with a shoulder 266 nm (for **7**). The absorptions in the range 430–800 nm with peaks at 538 and 696 nm (for **3**) are attributed to visible d–d transitions. As shown in Fig. S26, bpp demonstrates an intense peak at 276 nm in the UV range, which also corresponds to the π - π^* or n - π^* transition of the aromatic ring. However, complexes **4** and **5** exhibit UV absorption with maxima at 300 nm (for **4**) and 261, 306 and 375 nm (for **5**), which are a little bit different from that of the bpp linker, indicating that they may originate from an intraligand transition (ILCT) or metal to ligand charge-transfer transition (MLCT); but complex **6**, containing same ligand, shows a different absorption at 280 nm compared to complexes **4** and **5**. The absorption maximum of complex **6** is similar to the free bpp ligand, which proves in the d¹⁰ Zn system no MLCT is possible. The free 4-bpdb linker and complex **8** shows absorption maxima at 318 and 542 nm with a shoulder at 327 nm, respectively.

3.5. Luminescent properties

The luminescent properties of CPs with d¹⁰ metal centres have attracted much attention due to their potential applications as chemical sensors, in photochemistry and electroluminescence displays. The luminescence properties of complex **6** as well as the free bpp in the solid state were investigated at room temperature. The results are depicted in Fig. 5. Complex **6** and the bpp linker exhibit similar fluorescence emissions with bimodal bands at ca. 457/476 nm ($\lambda_{\text{ex}} = 280$ nm) and 468/486 nm ($\lambda_{\text{ex}} = 280$ nm), respectively. The ligand emission peaks may be attributed to π^* - n or π^* - π transitions. From the luminescence spectra, it is clear that complex **6** shows a totally N,N'-donor linker based blue shifted fluorescence compared to the bpp linker. It has been investigated that for d¹⁰ complexes, no emission originates from metal-centered MLCT/LMCT excited states, since d¹⁰ metal ions are difficult to reduce or oxidize [51,52]. So, it is concluded that the emission bands of complex **6** are exhibited due to intra-ligand electron transfer. In general, the enhancement of luminescent intensity is attributed to coordination of a ligand to a Zn(II) ion, which effectively increases the rigidity of the ligand and reduces thermal vibrations, thereby giving a reduction of energy loss by non-radiative decay [53–55].

4. Conclusion

Eight different coordination polymers (CPs) of transition metals based on 5-nitroisophthalate (nip^{2-}) with three different linear N,N'-donor dipyriddy linkers (4-bpdh, bpp and 4-bpdb) have been successfully synthesized by the slow diffusion technique at room

temperature, and characterized. Compounds **1–8** show fascinating 1D, 2D and 3D structures. Hydrogen-bonding and π – π stacking interactions contribute to the creation of the supramolecular architectures. A systematic study of the structural diversities of compounds **1–8** reveals that nip^{2-} can act as an excellent bridging ligand and display versatile coordination abilities, rather better than the unsubstituted isophthalate anion. The steric and electronic characteristics of the 5-positioned uncoordinated $-\text{NO}_2$ group of nip^{2-} play a crucial role in determining the dimensionality and topology of the final structure. In addition, the role of the N, N'-donor secondary ligands in the metal-carboxylate motif frequently directs structural changes and affords new network structures. In summary, this work gives a new promising route for constructing functional non-penetrating and interpenetrating networks with substituted polycarboxylate ligands and different N,N'-donor linkers to further develop the research field of crystal engineering.

Acknowledgments

Authors gratefully acknowledge the financial assistance given by SERB and CSIR India (Grant to D.G.). D.K.M. and B.B. acknowledge UGC for the senior research fellowship and A.D. acknowledges UGC for a Post Doctoral Fellowship for Women. The X-ray diffractometer facility under the DST-FIST program of Department of Chemistry (JU) is also gratefully acknowledged. Dr. K.K. Rajak of JU is gratefully acknowledged for the photoluminescence study.

Appendix A. Supplementary data

CCDC 1406207–1406214 contain the supplementary crystallographic data for complexes **1–8**. These data can be obtained free of charge via <http://www.ccdc.cam.ac.uk/conts/retrieving.html>, or from the Cambridge Crystallographic Data Centre, 12 Union Road, Cambridge CB2 1EZ, UK; fax: (+44) 1223-336-033; or e-mail: deposit@ccdc.cam.ac.uk. Supplementary data associated with this article can be found, in the online version, at <http://dx.doi.org/10.1016/j.poly.2015.10.052>.

References

- [1] B.F. Hoskins, R. Robson, *J. Am. Chem. Soc.* **111** (1989) 5962.
- [2] R. Robson, *J. Chem. Soc., Dalton Trans.* (2000) 3735.
- [3] M. O'Keefe, O.M. Yaghi, *Chem. Rev.* **112** (2012) 675.
- [4] O.K. Farha, J.T. Hupp, *Acc. Chem. Res.* **43** (2010) 1166.
- [5] F.A.A. Paz, J. Klinowski, S.M.F. Vilela, J.P.C. Tomé, J.A.S. Cavaleiro, J. Rocha, *Chem. Soc. Rev.* **41** (2012) 1088.
- [6] M. Li, D. Li, M.I. O'Keefe, O.M. Yaghi, *Chem. Rev.* **114** (2014) 1343.
- [7] E.V. Alexandrov, A.P. Shevchenko, A.A. Asiri, V.A. Blatov, *CrystEngComm* **17** (2015) 2913.
- [8] Q.R. Fang, D.Q. Yuan, J. Sculley, W.G. Lu, H.C. Zhou, *Chem. Commun.* **48** (2012) 254.
- [9] K. Jayaramulu, S.K. Reddy, A. Hazra, S. Balasubramanian, T.K. Maji, *Inorg. Chem.* **51** (2012) 7103.
- [10] P. Pachfule, B.K. Balan, S. Kurungot, R. Banerjee, *Chem. Commun.* **48** (2012) 2009.
- [11] R.B. Getman, Y.-S. Bae, C.E. Wilmer, R.Q. Snurr, *Chem. Rev.* **112** (2012) 703.
- [12] R.Q. Zou, H. Sakurai, Q. Xu, *Angew. Chem., Int. Ed.* **45** (2006) 2542.
- [13] D. Farrusseng, S. Aguado, C. Pinel, *Angew. Chem., Int. Ed.* **48** (2009) 7502.
- [14] B. Bhattacharya, D.K. Maity, P. Pachfule, E. Colacio, D. Ghoshal, *Inorg. Chem. Front.* **1** (2014) 414.
- [15] P. Mahata, S. Natarajan, P. Panissod, M. Drillon, *J. Am. Chem. Soc.* **131** (2009) 10140.
- [16] R. Dey, B. Bhattacharya, E. Colacio, D. Ghoshal, *Dalton Trans.* **42** (2013) 2094.
- [17] B.K. Tripuramallu, P. Manna, S.N. Reddy, S.K. Das, *Cryst. Growth Des.* **12** (2012) 777.
- [18] K. Liang, H.G. Zheng, Y.L. Song, M.F. Lappert, Y.Z. Li, X.Q. Xin, Z.X. Huang, J.T. Chen, S.F. Lu, *Angew. Chem., Int. Ed.* **43** (2004) 5776.
- [19] D.K. Maity, B. Bhattacharya, R. Mondal, D. Ghoshal, *CrystEngComm* **16** (2014) 8896.
- [20] Y. Cui, Y. Yue, G. Qian, B. Chen, *Chem. Rev.* **112** (2012) 1126.
- [21] B. Bhattacharya, R. Dey, D. Ghoshal, *J. Chem. Sci.* **125** (2013) 661.
- [22] B. Li, S.Q. Zang, C. Ji, H.W. Hou, C.W.M. Thomas, *Cryst. Growth Des.* **12** (2012) 1443.
- [23] X.T. Zhang, L.M. Fan, Z. Sun, W. Zhang, D.C. Li, J.M. Dou, L. Han, *Cryst. Growth Des.* **13** (2013) 792.
- [24] S.R. Zheng, Q.Y. Yang, R. Yang, M. Pan, R. Cao, C.Y. Su, *Cryst. Growth Des.* **9** (2009) 2341.
- [25] K.C. Xiong, F.L. Jiang, Y.L. Gai, Z.Z. He, D.Q. Yuan, L. Chen, K.Z. Su, M.C. Hong, *Cryst. Growth Des.* **12** (2012) 3335.
- [26] A.Y. Fu, Y.L. Jiang, Y.Y. Wang, X.N. Gao, G.P. Yang, L. Hou, Q.Z. Shi, *Inorg. Chem.* **49** (2010) 5495.
- [27] B. Liu, L.Y. Pang, L. Hou, Y.Y. Wang, Y. Zhang, Q.Z. Shi, *CrystEngComm* **14** (2012) 6246.
- [28] M. Du, X.J. Zhao, J.H. Guo, S.R. Batten, *Chem. Commun.* (2005) 4836.
- [29] S.T. Wu, L.S. Long, R.B. Huang, L.S. Zheng, *Cryst. Growth Des.* **7** (2007) 1746.
- [30] L.S. Long, *CrystEngComm* **12** (2010) 1354.
- [31] H.C. Fang, J.Q. Zhu, L.J. Zhou, H.Y. Jia, S.S. Li, X. Gong, S.B. Li, Y.P. Cai, P.K. Thallapally, J. Liu, G.J. Exarhos, *Cryst. Growth Des.* **10** (2010) 3277.
- [32] B. Zheng, H. Dong, J.F. Bai, Y.Z. Li, S.H. Li, M. Scheer, *J. Am. Chem. Soc.* **130** (2008) 7778.
- [33] G.X. Liu, H. Xu, H. Zhou, S. Nishihara, X.M. Ren, *CrystEngComm* **14** (2012) 1856.
- [34] L.F. Ma, L.Y. Wang, Y.Y. Wang, M. Du, J.G. Wang, *CrystEngComm* **11** (2009) 109.
- [35] H. Chun, *J. Am. Chem. Soc.* **130** (2008) 800.
- [36] J.H. Luo, M.C. Hong, R.H. Wang, R. Cao, L. Han, Z.Z. Lin, *Eur. J. Inorg. Chem.* (2003) 2705.
- [37] V.S.S. Kumar, F.C. Pigge, N.P. Rath, *New J. Chem.* **28** (2004) 1192.
- [38] A.J. Blake, N.R. Brooks, N.R. Champness, M. Crew, A. Deveson, D. Fenske, D.H. Gregory, L.R. Hanton, P. Hubberstey, M. Schroder, *Chem. Commun.* (2001) 1432.
- [39] Y.J. Qi, Y.H. Wang, C.W. Hu, M.H. Cao, L. Mao, E.B. Wang, *Inorg. Chem.* **42** (2003) 851.
- [40] A.R. Kennedy, K.G. Brown, D. Graham, J.B. Kirkhouse, M. Kittner, C. Major, C.J. McHugh, P. Murdoch, W.E. Smith, *New J. Chem.* **29** (2005) 826.
- [41] SMART (V 5.628), SAINT (V 6.45a), XPREP, SHELXTL, Bruker AXS Inc., Madison, WI, 2004.
- [42] G.M. Sheldrick, *SADABS* (Version 2.03), University of Göttingen, Germany, 2002.
- [43] G.M. Sheldrick, *SHELXS-97*, *Acta. Crystallogr. A* **64** (2008) 112.
- [44] A.L. Spek, *Acta. Crystallogr. D* **65** (2009) 148.
- [45] L.J. Farrugia, *J. Appl. Crystallogr.* **30** (1997) 565.
- [46] L.J. Farrugia, *WinGX, J. Appl. Crystallogr.* **32** (1999) 837.
- [47] V.A. Blatov, A.P. Shevchenko, V.N.J. Serezhkin, *Appl. Crystallogr.* **33** (2000) 1193.
- [48] V.A. Blatov, L. Carlucci, G. Ciani, D.M. Proserpio, *CrystEngComm* **6** (2004) 377.
- [49] S. Ohkoshi, H. Tokoro, T. Hozumi, Y. Zhang, K. Hashimoto, C. Mathonière, I. Bord, G. Rombaut, M. Verelst, C.C. Moulin, F. Villain, *J. Am. Chem. Soc.* **128** (2006) 270.
- [50] J.H. Wang, Y.Q. Fang, L. Bourget-Merle, M.I.J. Polson, G.S. Hanan, A. Juris, F. Loiseau, S. Campagna, *Chem. Eur. J.* **12** (2006) 8539.
- [51] L. Wen, Y. Li, Z. Lu, J. Lin, C. Duan, Q. Meng, *Cryst. Growth Des.* **6** (2006) 530.
- [52] L.-P. Zhang, J.-F. Ma, J. Yang, Y.-Y. Pang, J.-C. Ma, *Inorg. Chem.* **49** (2010) 1535.
- [53] J. Zhang, Y.R. Xie, Q. Ye, R.G. Xiong, Z. Xue, X.Z. You, *Eur. J. Inorg. Chem.* (2003) 2572.
- [54] L.L. Wen, D.B. Dang, C.Y. Duan, Y.Z. Li, Z.F. Tian, Q.J. Meng, *Inorg. Chem.* **44** (2005) 7161.
- [55] Y. Jia, H. Li, Q. Guo, B. Zhao, Y. Zhao, H. Hou, Y. Fan, *Eur. J. Inorg. Chem.* (2012) 3047.